Chemical vapor deposition synthesis and terahertz photoconductivity of low-bandgap *N* = 9 armchair graphene nanoribbons

Zongping Chen[1], Hai I. Wang[2], Joan Teyssandier[3], Kunal S. Mali[3], Tim Dumslaff[1], Ivan Ivanov[1], Wen Zhang[1], Pascal Ruffieux[4], Roman Fasel[4,5], Hans Joachim Räder[1], Dmitry Turchinovich[1], Steven De Feyter[3], Xinliang Feng[6], Mathias Kläui[2], Akimitsu Narita*[,1], Mischa Bonn*[,1] and Klaus Müllen*[,1,7]

[1]Max Planck Institute for Polymer Research, Ackermannweg 10, D-55128 Mainz, Germany

[2]Institute of Physics, Johannes Gutenberg-University Mainz, Staudingerweg 7, 55128 Mainz, Germany

[3]Division of Molecular Imaging and Photonics, Department of Chemistry, KU Leuven Celestijnenlaan, 200 F, B-3001 Leuven, Belgium

[4]Empa, Swiss Federal Laboratories for Materials Science and Technology, nanotech@surfaces Laboratory, 8600 Dübendorf, Switzerland

[5]Department of Chemistry and Biochemistry, University of Bern, 3012 Bern, Switzerland

[6]Center for Advancing Electronics Dresden and Department of Chemistry and Food Chemistry, Technische Universität Dresden, Mommsenstrasse 4, D-01062 Dresden, Germany

[7]Institute of Physical Chemistry, Johannes Gutenberg-University Mainz, Duesbergweg 10-14, 55128 Mainz, Germany

Supporting Information Placeholder

ABSTRACT: Recent advances in bottom-up synthesis of atomically defined graphene nanoribbons (GNRs) with various microstructures and properties have demonstrated their promise in electronic and optoelectronic devices. Here we synthesize *N* = 9 armchair graphene nanoribbons (9-AGNRs) with a low optical bandgap of ~1.0 eV and extended absorption into the infrared range by an efficient chemical vapor deposition process. Time resolved terahertz spectroscopy has been employed to characterize the photoconductivity in 9-AGNRs, and revealed their high intrinsic charge-carrier mobility of approximately 350 $cm^2 \cdot V^{-1} \cdot s^{-1}$.

Graphene nanoribbons (GNRs), quasi-one-dimensional graphene strips, have attracted much attention as a new class of semiconducting materials for various applications in electronic and optoelectronic devices.[1-6] In the past few years, various types of GNRs have been synthesized via bottom-up approaches in solution as well as on metal surfaces[3-11] with a wide range of bandgap energies. Among the different bottom-up methods, on-surface synthesis, especially through chemical vapor deposition (CVD) appears to be highly promising, as being capable of high-throughput and scalable growth of structurally defined GNRs at low cost.[6, 8, 12] The surface-grown GNR films can be readily transferred onto arbitrary substrates, allowing for optical characterizations and device integration. However, the performance of field-effect transistor (FET) devices fabricated with such GNRs have so far been compromised by a huge contact resistance,[6, 8, 10, 12-13] hampering the investigations of their intrinsic electronic transport properties.

For efficient optoelectronic applications such as photovoltaics, GNRs with an optical bandgap between 1.0 to 1.3 eV are fundamentally important, which is expected to provide GNR-based devices approaching the Shockley–Queisser limit.[14] Nevertheless, structurally well-defined GNRs with optical bandgaps in this range still remain rather rare.[5] The electronic structure of armchair GNRs (n-AGNRs) has been shown to be extremely sensitive to the ribbon width, and can be divided into three subfamilies with atomic number N = 3n, 3n + 1, and 3n + 2 (n = 1, 2, 3, ...). All three kinds of AGNRs are expected to be semiconducting. And the bandgap of different subfamily AGNRs with the same n varies as: 3n + 2 < 3n < 3n + 1.[1-2] According to theoretical prediction by *GW*-BSE calculations, *N* = 9 armchair graphene nanoribbons (9-AGNRs) possess an optical bandgap of ~1.0 eV,[15] which was very recently corroborated by the solution-mediated synthesis reported by Dong *et al.*[16] On the other hand, Nakae *et al.* previously proposed a synthesis of 9-AGNRs by a low-pressure CVD method,[12] but the observed optical bandgap was larger, and unambiguous structural characterization has remained elusive.

Here we report an efficient CVD process for inexpensive high-throughput growth of structurally defined 9-AGNRs. The obtained 9-AGNRs exhibit a low optical bandgap of ~1.0 eV with broad absorption up to ~1200 nm. Ultrafast optical pump - THz probe spectroscopy (OPTP) is for the first time applied to surface-synthesized GNRs, revealing high intrinsic charge-carrier mobility of 9-AGNRs, i.e., approximately 350

$cm^2 \cdot V^{-1} \cdot s^{-1}$, which reflects the high quality of the sample fabricated by our CVD method. The potential of 9-AGNRs for future optoelectronics has been further demonstrated in comparison with previously reported 7-AGNRs and chevron-type GNRs, showing higher photoconductivity by a factor of 1.2 and 2.5, respectively.

We have recently reported an efficient ambient-pressure CVD growth of 7-AGNRs and chevron-type GNRs.[6] Notably, the CVD-grown GNRs demonstrated structural perfection well comparable with GNRs synthesized under ultra-high-vacuum conditions. Because of the high versatility, our CVD process provides access to a broad class of GNRs with designed structures, by employing different oligophenylene monomers. The synthesis of 9-AGNRs has been achieved by CVD using 3',6'-dibromo-1,1':2',1''-terphenyl (**DBTP**) as the monomeric building block (Figure 1). In a typical CVD experiment, **DBTP** is sublimed at 135-150 °C and deposited on the Au/mica substrate kept at 200 °C. At this temperature **DBTP** is simultaneously dehalogenated, generating biradicals that subsequently undergo a coupling reaction to form oligo(diphenyl-*p*-phenylene) (**ODPP**) with a linear backbone (Figure 1a). The sample is subsequently annealed at a higher temperature of 400 °C to transform **ODPPs** into 9-AGNRs through the surface-assisted intramolecular cyclodehydrogenation, eliminating 8 hydrogens per repeating unit.

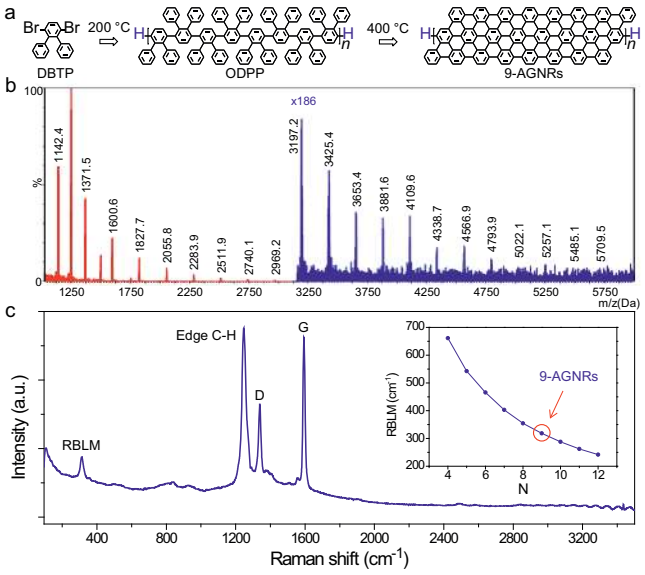

Figure 1. (a) Synthesis of 9-AGNRs by CVD method. (b) Mass spectrum of **ODPPs** before cyclodehydrogenation. (c) Raman spectrum of CVD-grown 9-AGNRs by 785 nm laser. The calculated RBLM peaks vs. width of GNRs are given in the inset.[17]

To investigate the chemical structures of the oligomer/polymer after the radical polymerization step during the on-surface synthesis of GNRs, we have recently developed a quick and powerful surface-mass-spectrometry analysis method.[6] **ODPPs** were thus studied by the high-resolution matrix-assisted laser desorption/ionization time-of-flight mass spectrometry (MALDI-TOF MS) with *trans*-2-[3-(4-*tert*-butylphenyl)-2-methyl-2-propenylidene] malononitrile (**DCTB**) as matrix (Figure 1b). The MS spectrum of the **ODPPs** exhibits regular patterns from pentamer (m/z = ~1142 Da) up to a species with 23 units (m/z = ~5257 Da). The difference between the neighboring signals is exactly the same value of ~228 Da, which corresponds to the molecular mass of the repeating unit. The observed isotopic distribution of the **ODPPs** is in agreement with the simulated pattern, demonstrating the successful polymerization reaction to form the expected structures (Figure S1).

The Raman spectrum of the final 9-AGNRs after cyclodehydrogenation reveals four main peaks at 1592, 1340, 1250, and 315 cm^{-1}, which can be assigned to G, D, Edge C-H, and radial breathing-like mode (RBLM) peaks, respectively (Figures 1c and S2).[18] The sharp and intense width-specific RBLM peak is in excellent agreement with the DFT calculation, demonstrating the high uniformity in width of the obtained 9-AGNR sample (inset of Figure 1c).[17] Note that the specific RBLM peak of 9-AGNRs was not observed in previous reports on 9-AGNRs by CVD growth and solution synthesis.[12, 16] The monolayers of as-synthesized 9-AGNRs were further unambiguously characterized using atomic force microscopy (AFM) as well as scanning tunneling microscopy (STM) under ambient conditions (Figures 2 and S3). AFM height images show terraces of Au(111) surface uniformly covered with monolayer thick (~2.5 Å) film of 9-AGNRs (Figure 2a). STM images agree well with AFM data indicating good surface coverage of striped features (Figure 2b). Typical domain size is ~30 nm. Each terrace of Au(111) contains multiple domains of 9-AGNRs indicating several nucleation sites along each terrace. Well-defined domains of planar striped features are sometimes surrounded by ill-defined regions which may indicate adsorption of unreacted material. The width of each striped feature is ~1.2 nm and it is uniform across the surface (Figure 2c, d). This is in good agreement with the expected width of 9-AGNRs estimated from a molecular mechanics model (Figure 2e) and further indicates that the 9-AGNRs remain parallel (face-on) to the Au(111) surface. The 9-AGNRs appear continuous and close-packed within each domain. While the STM images provided in Figure 2 reveal GNRs with length up to ~20 nm, the length can reach up to 30-35 nm (see Figure S3).

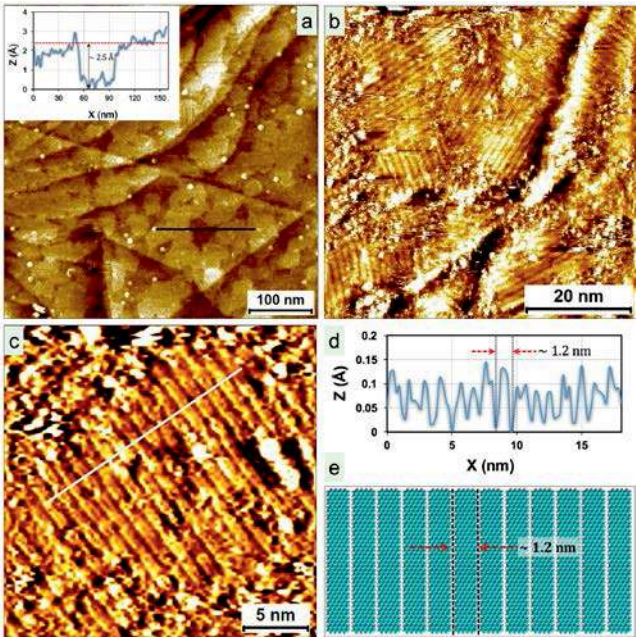

Figure 2. AFM/STM characterization of 9-AGNRs on Au(111)/Mica surface. (a) AFM height image showing domains of 9-AGNRs. The inset shows height profile along the black line, indicating formation of monolayer of 9-AGNRs.

(b) STM image showing domains of 9-AGNRs. (I_{set} = 300 pA; V_{bias} = 0.06 V) (c) Small-scale STM image showing 9-AGNRs as well-defined stripes with uniform width of ~1.2 nm. (I_{set} = 60 pA; V_{bias} = 0.03 V) (d) Line profile along the white line in panel (c). (e) Molecular model showing the laterally stacked 9-AGNRs.

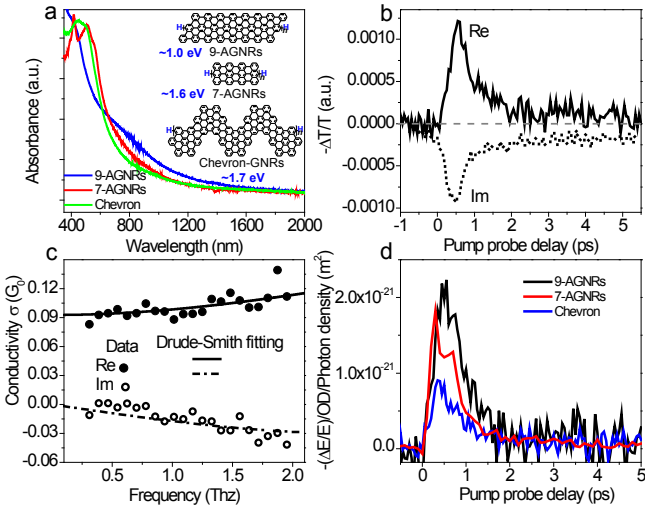

Figure 3. (a) UV-vis-NIR absorption spectra of different CVD-grown GNRs. The inset shows the chemical structures of the GNRs and their optical bandgaps. (b) Time-resolved photoinduced real and imaginary conductivity of 9-AGNRs measured as the relative change of THz transmission at the peak of THz pulse (real, solid line) and zero-crossing point of THz pulse (imaginary, dotted line) (pump at 400 nm, with fluence 200 μJ/cm²). (c) Frequency-resolved THz conductivity of 9-AGNRs measured at the peak of the photoconductivity, and a Drude-Smith fit with c parameter ~-0.72 ± 0.02. (d) Comparative study of THz photoconductivities of different GNR structures.

After the growth, the 9-AGNRs can be readily transferred to other substrates, yielding a large-area uniform GNR film, as demonstrated by the optical images and Raman mapping (Figure S4). The UV-vis-NIR absorption analysis of the 9-AGNRs was carried out by multiple transfer of 9-AGNR films on one fused silica substrate to have enough optical density (Figure 3a). An absorption onset was thus detectable at ~1185 nm in the IR region, suggesting an optical bandgap of ~1.0 eV for the obtained 9-AGNR multilayer film, which is close to the theoretical value of isolated 9-AGNR,[15] and significantly smaller than values of 7-AGNRs (~1.6 eV) and chevron-type GNRs (~1.7 eV) (see Figures 3a and S5).

For assessing the potential of the 9-AGNRs for optoelectronics, we have investigated their photoconductivity by OPTP,[19] which has been demonstrated as a powerful spectroscopic tool for contact-free and noninvasive characterization of the intrinsic charge-carrier mobility within individual solution-synthesized GNRs.[4-5, 20] In Figure 3b, we show the time-resolved photoconductivity dynamics (in a form of transient change of the THz transmission) of a thin film of 25 layers of 9-AGNRs deposited on fused silica. After photoexcitation with the optical pulse (400 nm wavelength), we observe a sub-picosecond rapid rise and a subsequent, ~2 ps - fast decay in the real conductivity. The imaginary conductivity component displays a similarly fast rise-time, however the decay time is considerably longer. Both the transient conductivity dynamics and their time scale are fully consistent with our previous studies on solution-synthesized GNRs in dispersions[4-5, 20] and can be rationalized by the charge state transitions from quasi-free cases at early time (< 1 ps) to strongly bounded excitons at the longer time-delays (> 2 ps with long-lived imaginary conductivity indicative of photoinduced dielectric polarizability of the sample). Furthermore, the frequency-dependent THz conductivity at the peak position of the dynamics shown in Figure 3b (~0.55 ps after photoexcitation), is demonstrated in Figure 3c. We observe a positive real and negative imaginary component with both amplitudes increasing with the frequencies, sharing a large similarity with the frequency-resolved THz conductivity in semiconducting polymers[21-23] and other types of GNRs dispersed in organic solvents.[4] The Drude-Smith model[24] has been widely employed to model the transport characteristic in conducting polymers and GNRs as:

$$\sigma_{DS} = \frac{\varepsilon_0 \omega_p^2 \tau}{1 - i\omega\tau}\left(1 + \frac{c}{1 - i\omega\tau}\right)$$

Here, ε_o is the vacuum permittivity, ω_p is the plasma frequency (which is proportional to the carrier concentration), τ is the electron momentum scattering time, and the parameter c accounts for the correlation between carrier momentum before and after a scattering event, with c = 0 as non-preferential, fully isotropic scattering (classical Drude model of free electron plasma) and c = −1 as backscattering-dominant process of localized charge carrier. By fitting the complex conductivity using the Drude-Smith model as shown in Figure 3c, we can obtain c parameter ~-0.72 ± 0.02, which is fully consistent with previous reported c values in randomly oriented 1D Drude conductors, such as carbon nanotubes and GNRs in dispersions.[20] Based on the fitting, we can also derive the momentum scattering time to be 20 ± 5 fs. Applying the reported effective mass for the 9-AGNRs (m^* = 0.1·m_0),[10] one can readily estimate the intrinsic dc carrier mobility in 9-AGNRs using $\mu = e\tau/m^*$, which results in a value of 352 ± 88 $cm^2 \cdot V^{-1} \cdot s^{-1}$. This is a rough estimation of the local carrier mobility within a nanoribbon. The physical length of the molecular wire has been reported to affect its charge mobility due to the charge scattering effect at the ends of the molecular wires.[25] Consequently, controlling the growth conditions for producing even longer 9-AGNRs than those reported here (up to ~35 nm) could be beneficial for further boosting the high-frequency carrier mobility of 9-AGNRs for device applications. Speaking of the measured photoconductivity of the sample, we can also estimate carrier mobility in the film of 25 layers of GNR networks – a film of GNR chains intricately connected with each other. This can be estimated from average measured conductivity and the quantum yield (which in the similar materials are found to be QE = 10^{-3}–10^{-5}).[22] Thus, the mobility in the film is comparable to 50–5000 $cm^2 \cdot V^{-1} \cdot s^{-1}$, which indicates the high quality of the CVD-grown GNRs used in this study. We expect a negligible effect of sample thickness on the mobility estimate for samples consisting of a large number of layers, such as 25 layers in this study (see Supporting Information for extended discussion). Note that this intrinsic charge-carrier mobility estimated for 9-AGNRs is much higher than the mobility measured in FET devices on thin films of 7-AGNRs and chevron-type GNRs (estimated to be ~10^{-3}-10^{-5} $cm^2 V^{-1} s^{-1}$),[6, 12] since the electrical response in the GNR FET devices is mostly dominated by the large inter-GNR junction resistances as

well as the contact resistance between the GNRs and the electrodes.

To establish the potential of 9-AGNRs for optoelectronic applications, we have conducted a further comparative investigation of photoconductivity for two other CVD-grown GNRs with certain structural similarities: namely, 7-AGNRs and chevron-type GNRs (see Figure 3a). By selectively exciting the samples with a fixed pump fluence at 400 nm, we have compared the photon-induced THz conductivity for all three GNR structures as shown in Figure 3d. As we can see, for a given excitation fluence and optical density (OD), the photoconductivity of 9-AGNRs is a factor of 1.2 and 2.5 higher than that of 7-AGNRs and chevron-type GNRs, respectively, which can be partially attributed to the relatively smaller electron effective mass, leading to a higher mobility, of 9-AGNRs than that of the rest GNRs.[10, 26-27]

In summary, a synthesis of structurally well-defined 9-AGNRs has been achieved through a highly efficient CVD method. STM, Raman, UV-vis-NIR absorption, and time resolved THz spectroscopy analysis manifested the high quality of the 9-AGNRs with a low bandgap of ~1.0 eV and absorption extending up to ~1200 nm. Given the scalability and low cost of the CVD synthetic method, these results pave the way for exploiting such bottom-up synthesized GNRs for efficient optoelectronic device applications, including visible - to - infrared photodetectors and photovoltaics.

ASSOCIATED CONTENT

Supporting Information

Experimental details and more characterization data: MALDI-TOF MS, Raman spectra and AFM/STM images.
The Supporting Information is available free of charge on the ACS Publications website at DOI: .

AUTHOR INFORMATION

Corresponding Author

*narita@mpip-mainz.mpg.de
*bonn@mpip-mainz.mpg.de
*muellen@mpip-mainz.mpg.de

Notes

The authors declare no competing financial interests.

ACKNOWLEDGMENT

This work was financially supported by DFG Priority Program Graphene SPP 1459, the Max Planck Society, the Office of Naval Research BRC Program, the Swiss National Science Foundation, and the European Commission through the FET-Proactive Project "MoQuaS" (FP7-ICT-2013-10, contract number 610449), EU CIG (334324 LIGHTER), and Graphene Flagship.

REFERENCES

(1) Yang, L.; Park, C. H.; Son, Y. W.; Cohen, M. L.; Louie, S. G. Phys. Rev. Lett. 2007, 99, 186801.
(2) Son, Y. W.; Cohen, M. L.; Louie, S. G. Phys. Rev. Lett. 2006, 97, 216803.
(3) Cai, J. M.; Ruffieux, P.; Jaafar, R.; Bieri, M.; Braun, T.; Blankenburg, S.; Muoth, M.; Seitsonen, A. P.; Saleh, M.; Feng, X. L.; Müllen, K.; Fasel, R. Nature 2010, 466, 470-473.
(4) Narita, A.; Feng, X.; Hernandez, Y.; Jensen, S. A.; Bonn, M.; Yang, H.; Verzhbitskiy, I. A.; Casiraghi, C.; Hansen, M. R.; Koch, A. H.; Fytas, G.; Ivasenko, O.; Li, B.; Mali, K. S.; Balandina, T.; Mahesh, S.; De Feyter, S.; Müllen, K. Nature Chem. 2014, 6, 126-132.
(5) Narita, A.; Verzhbitskiy, I. A.; Frederickx, W.; Mali, K. S.; Jensen, S. A.; Hansen, M. R.; Bonn, M.; De Feyter, S.; Casiraghi, C.; Feng, X.; Müllen, K. ACS Nano 2014, 8, 11622-11630.
(6) Chen, Z.; Zhang, W.; Palma, C.-A.; Lodi Rizzini, A.; Liu, B.; Abbas, A. N.; Richter, N.; Martini, L.; Wang, X.-Y.; Cavani, N.; Lu, H.; Mishra, N.; Coletti, C.; Berger, R.; Klappenberger, F.; Kläui, M.; Candini, A.; Affronte, M.; Zhou, C.; De Renzi, V.; del Pennino, U.; Barth, J. V.; Räder, H. J.; Narita, A.; Feng, X.; Müllen, K. J. Am. Chem. Soc. 2016, 138, 15488-15496.
(7) Ruffieux, P.; Wang, S.; Yang, B.; Sánchez-Sánchez, C.; Liu, J.; Dienel, T.; Talirz, L.; Shinde, P.; Pignedoli, C. A.; Passerone, D.; Dumslaff, T.; Feng, X.; Müllen, K.; Fasel, R. Nature 2016, 531, 489-492.
(8) Sakaguchi, H.; Song, S.; Kojima, T.; Nakae, T. Nature Chem. 2017, 9, 57-63.
(9) Narita, A.; Wang, X. Y.; Feng, X. L.; Müllen, K. Chem. Soc. Rev. 2015, 44, 6616-6643.
(10) Talirz, L.; Ruffieux, P.; Fasel, R. Adv. Mater. 2016, 28, 6222-6231.
(11) Talirz, L.; Söde, H.; Dumslaff, T.; Wang, S.; Sanchez-Valencia, J. R.; Liu, J.; Shinde, P.; Pignedoli, C. A.; Liang, L.; Meunier, V.; Plumb, N. C.; Shi, M.; Feng, X.; Narita, A.; Müllen, K.; Fasel, R.; Ruffieux, P. ACS Nano 2017, DOI: 10.1021/acsnano.1026b06405.
(12) Sakaguchi, H.; Kawagoe, Y.; Hirano, Y.; Iruka, T.; Yano, M.; Nakae, T. Adv. Mater. 2014, 26, 4134-4138.
(13) Bennett, P. B.; Pedramrazi, Z.; Madani, A.; Chen, Y. C.; de Oteyza, D. G.; Chen, C.; Fischer, F. R.; Crommie, M. F.; Bokor, J. Appl. Phys. Lett. 2013, 103, 253114.
(14) Shockley, W.; Queisser, H. J. J. Appl. Phys. 1961, 32, 510-519.
(15) Prezzi, D.; Varsano, D.; Ruini, A.; Marini, A.; Molinari, E. Phys. Rev. B 2008, 77, 041404.
(16) Li, G.; Yoon, K.-Y.; Zhong, X.; Zhu, X.; Dong, G. Chem.-Eur. J. 2016, 22, 9116-9120.
(17) Zhou, J.; Dong, J. Appl. Phys. Lett. 2007, 91, 173108.
(18) Saito, R.; Furukawa, M.; Dresselhaus, G.; Dresselhaus, M. S. J. Phys.: Condens. Matter 2010, 22, 334203.
(19) Ulbricht, R.; Hendry, E.; Shan, J.; Heinz, T. F.; Bonn, M. Rev. Mod. Phys. 2011, 83, 543-586.
(20) Jensen, S. A.; Ulbricht, R.; Narita, A.; Feng, X.; Müllen, K.; Hertel, T.; Turchinovich, D.; Bonn, M. Nano Lett 2013, 13, 5925-5930.
(21) Cunningham, P. D.; Hayden, L. M. J. Phys. Chem. C 2008, 112, 7928-7935.
(22) Hendry, E.; Koeberg, M.; Schins, J. M.; Nienhuys, H. K.; Sundström, V.; Siebbeles, L. D. A.; Bonn, M. Phys. Rev. B 2005, 71, 125201.
(23) Hendry, E.; Schins, J. M.; Candeias, L. P.; Siebbeles, L. D. A.; Bonn, M. Phys. Rev. Lett. 2004, 92, 196601.
(24) Smith, N. V. Phys. Rev. B 2001, 64, 155106.
(25) Prins, P.; Grozema, F. C.; Schins, J. M.; Patil, S.; Scherf, U.; Siebbeles, L. D. A. Phys. Rev. Lett. 2006, 96, 146601.
(26) Raza, H.; Kan, E. C. Phys. Rev. B 2008, 77, 245434.
(27) Bronner, C.; Haase, A.; Tegeder, P. Phys. Rev. B 2015, 91, 045428.

Table of Contents